TOWARDS A BETTER REPRESENTATION OF HIGH DENSITY ICE PARTICLES IN A STATE-OF-THE-ART TWO-MOMENT BULK MICROPHYSICAL SCHEME

Ulrich Blahak*
Institut für Meteorologie und Klimaforschung, Universität Karlsruhe / Forschungszentrum Karlsruhe

1 INTRODUCTION

One of the upcoming topics in cloud microphysics is to investigate the influence of increased air pollution by anthropogenic aerosols on the evolution of convective clouds and formation of hail in midlatitude storms. In this context, it is of importance that the cloud microphysical scheme is able to predict the evolution of hail with a certain degree of confidence. Hail particles may influence the microphysical-dynamical feedback and the simulated precipitation efficiency due to their ability for efficient collision and riming growth and high sedimentation velocity.

Originally, the 2-moment bulk microphysical scheme by Seifert and Beheng (2006) with the modifications given in Seifert et al. (2006), henceforth called "bulk scheme", comprised the 5 hydrometeor categories cloud water, rain water, cloud ice, snow and graupel. It predicts the first 2 moments of the underlying particle size distribution with respect to particle mass, namely the number- and mass density, for each of the hydrometeor classes. In principal, this enables a more realistic simulation of most cloud microphysical processes (e.g., collision/coalescence, accretion, sedimentation, evaporation) compared to conventional 1-moment schemes. In contrast to other 2-moment schemes, a new detailed parameterization of warm rain processes (autoconversion, accretion, selfcollection) is applied as well as a very careful treatment of all other collision processes (solid-solid and liquid-solid). E.g., collision processes between ice species take into account a variation of the fallspeed for particles of a given size. Moreover, the scheme is able to take into account different aerosol regimes (high-CCN versus low-CCN conditions).

Recently, the Seifert-Beheng-scheme (referred to as two-moment scheme in the following) has been revised with respect to a better representation of high density ice particles like hail. These revisions are motivated (sections 2 and 3) and described (section 5) in the following.

2 FORMATION OF HAIL PARTICLES

According to the WMO definition, a hailstone is a high-density ice particle with a diameter larger than 5 mm. It is known that such particles originate preferably in the updraft regions of convective clouds. Here, freezing raindrops or other dense ice hydrometeors might serve as initial "hail embryos" which subsequently grow by accretion of supercooled water droplets (riming) and maintain a rather high particle bulk density ρ_b during their growth, accompanied by a comparatively high particle fall speed. However, usually such particles cannot grow to large dense hailstones with sizes of up to several cm through riming alone. An important mechanism leading to large hail is the recirculation of falling and probably partially melting hailstones into an adjacent strong updraft with subsequent refreezing and further growth by riming, leading to the often observed concentrically layered structure of hail stones.

A further mechanism to create larger sized dense ice particles is the conversion of large graupel into a high density particle by the so called "wet growth" process. If the graupel particle under consideration is located in an environment with large concentration of supercooled liquid water, it exhibits a high riming rate and a large release of latent heat of freezing. Initially this latent heat is stored within the growing graupel particle, increases its heat content and temperature and is transported away from the particle by turbulent heat transfer. In a steady state environment the growing particle would reach a steady temperature as equilibrium between latent heat release on and heat flux away from the particle. If this temperature T_S reaches 0°C, no more freezing of supercooled water can occur (Schumann-Ludlam limit, e.g., Young, 1993). Instead, liquid water accumulates on the particle and/or gets soaked into pores and air inclusions of the growing particle. Moreover, excess heat now is used to melt the ice core. It is said that the particle has reached the "wet growth regime" and transforms into a higher density particle, which eventually may refreeze completely later. Theoretical considerations show (e.g., Dennis and Musil, 1973) that, at given environmental supercooled water content and temperature, particles are in wet growth mode if their diameter D exceeds a certain threshold diameter D_{wg}. Particles having $D > D_{wg}$ are in wet growth mode, smaller particles are not. Besides the increased bulk density, a particle in wet growth mode more efficiently grows by accretion of ice particles since its sticking efficiency is near unity in contrast to lower values for dry particles.

3 PREVIOUS REPRESENTATION OF HIGH DENSITY ICE PARTICLES

As mentioned above, the two-moment scheme in its initial version comprised 5 classes of hydrometeors, namely cloud drops, rain, cloud ice, snow and graupel. It did not contain a hail-like class of high density particles with a distinctively large fall speed. There was only the abovementioned class of graupel particles which exhibited an "intermediate" bulk density and fallspeed. The corresponding size-mass and fallspeed-mass relations are specified in the bulk scheme in the usual form of simple two-parametric power laws

$$D = a_g x^{b_g} \quad , \quad v = a_v x^{b_v} \tag{1}$$

with parameters a_g, b_g, a_v and b_v and particle mass x. The above original graupel class was specified in a way that $\rho(D)$ increased from rather small values of 300 kg m^{-3} for $D = 1$ mm to about 600 kg m^{-3} at $D = 8$ mm. Fallspeed increased from about 1 m s^{-1} for $D = 1$ mm to about 8 m s^{-1} at $D = 8$ mm. Graupel was initiated by riming of snow and cloud ice as well as by freezing of raindrops. This seems inappropriate to realistically represent hail.

*Corresponding author address: Ulrich Blahak, Institut für Meteorologie und Klimaforschung, Universität Karlsruhe / Forschungszentrum Karlsruhe, Postfach 3640, D-76021 Karlsruhe, Germany;
e-mail: ulrich.blahak@imk.fzk.de.

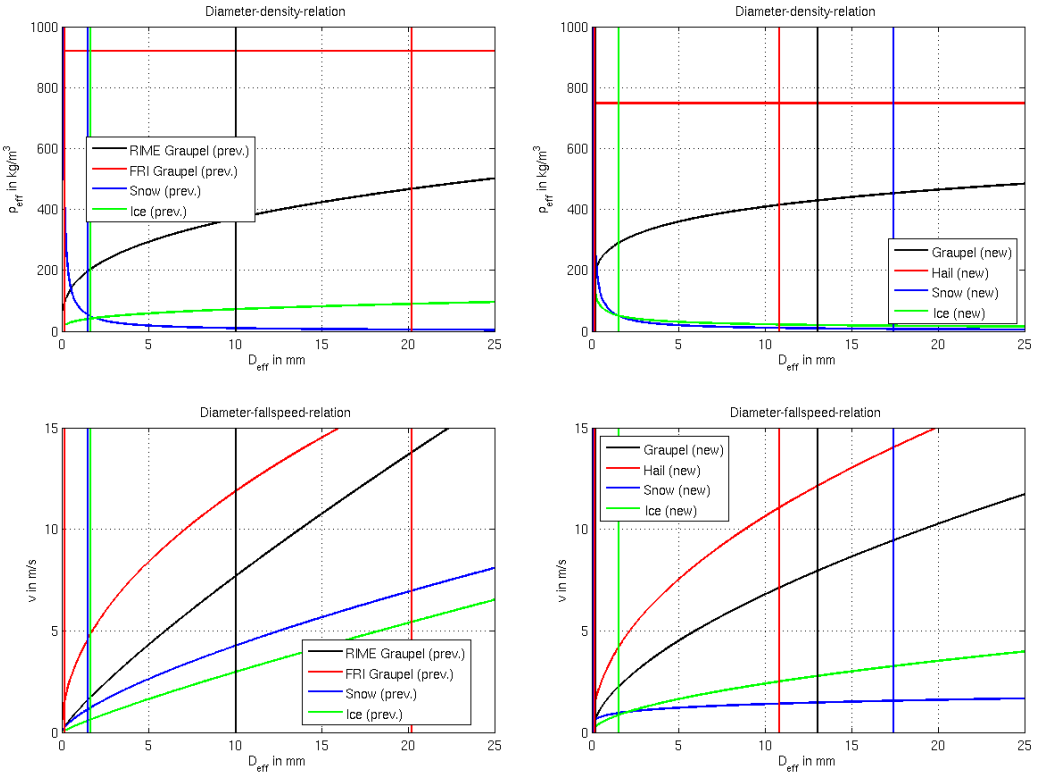

Fig. 1: Diameter-density- and diameter-fallspeed-relations for the ice hydrometeor types of the previous version of the bulk scheme (left column) and the new version (right column). Spherical equivalent particle diameter D (denoted by D_{eff} in the figures) is in mm, bulk density ρ in $kg\,m^{-3}$ and fallspeed v in $m\,s^{-1}$. Vertical lines denote minimum and maximum allowed mean mass diameters D_M (if D_M is outside this range at a certain grid box, number density is changed in a way to clip D_M to this allowed range).

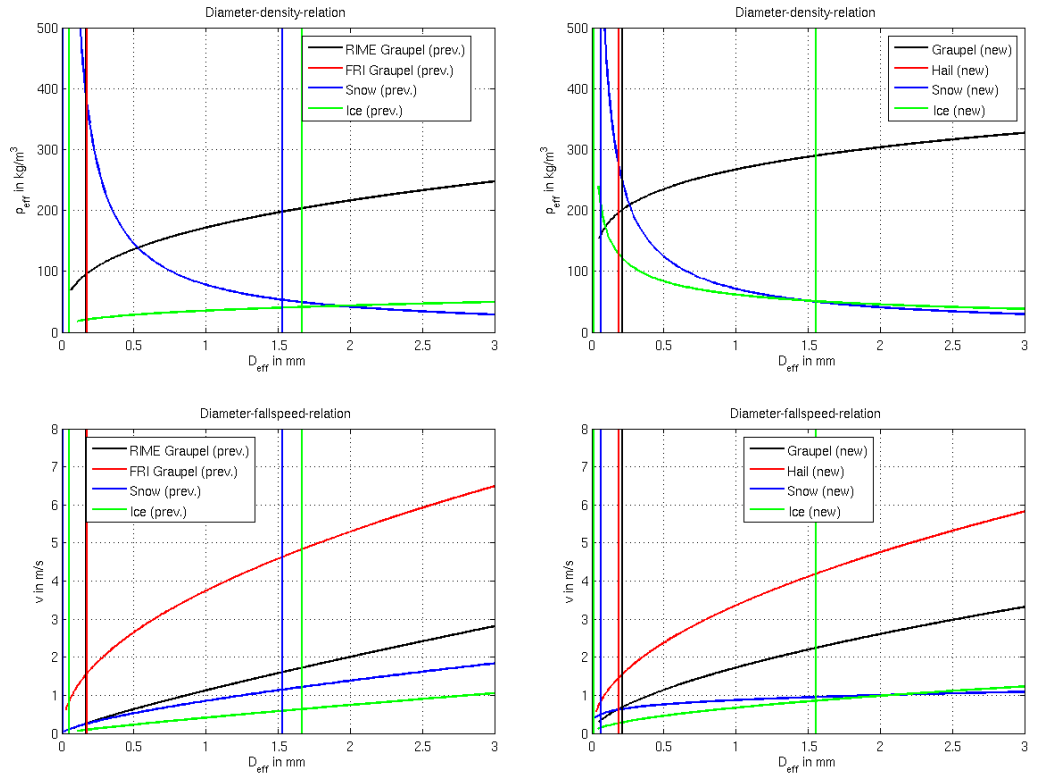

Fig. 2: Same as Figure 1, but diameter range zoomed in to values smaller than 3 mm.

As a first step, the graupel class has been split into two classes according to its formation process. Graupel particles originating from riming of snow and ice were retained in a class of rather low bulk density and fallspeed (RIME Graupel), and those particles initiated by freezing of raindrops have been put into a graupel class with bulk density and fallspeed resembling solid ice spheres (FRI Graupel). The bulk density and fall speed of these two graupel classes as well as those of snow and cloud ice are depicted in Figure 1, left column (full size range up to $D = 25$ mm) and Figure 2, left column (zoomed in to small sizes up to $D = 3$ mm). Vertical lines represent the minimum and maximum allowed mean mass diameters D_M,

$$D_M = a_g \left(\frac{Q}{N}\right)^{b_g} = \left(\frac{6}{\pi \rho_b} \frac{L}{N}\right)^{\frac{1}{3}} \quad . \tag{2}$$

ρ_b denotes bulk density, Q and N are mass- and number densities of the corresponding hydrometeor species. FRI-graupel is allowed to interact with other hydrometeors exactly in the same way as the previous single graupel class, except collisions between the two graupel classes are not considered (collision efficiency of 0 assumed). More details can be found in Noppel et al. (2006).

With the implementation of the FRI-graupel class it was hoped to be able to simulate more realistically the commonly higher sedimentation velocity and accretional growth of high density ice particles, which enables them to grow bigger and "survive" a larger fall distance at temperature above freezing. More of these high density particles are expected to "make it" to the ground as compared to the original version of the scheme.

However, due to the lack or imperfection of certain process parameterizations like melting, shedding of melt water, refreezing of a wet particle and wet growth, it was not expected to reflect the processes of wet growth and recirculation in a realistic way. Note that the added higher density FRI-graupel class has not yet been termed "hail". With this scheme (henceforth "previous" or "old" scheme), a test case has been simulated using the COSMO model of the German Weather service (DWD), which will be presented in the next section.

4 RESULTS OF THE PREVIOUS TWO-MOMENT-SCHEME VERSION — IDENTIFIED FEATURES AND DEFICIENCIES

The above two-moment-scheme-version with the two splitted graupel classes has been tested using different idealized test cases. One of these test cases will be presented here. Simulations have been carried out with a test version of the nonhydrostatic, fully compressible COSMO model of the German Weather Service (DWD). The characteristics of the simulations are:

- COSMO model version 3.19
- Two-dimensional setup (X-Z-plane)
- $\Delta X = 350$ m, $\Delta Z = 125$ m, 485 grid points in X-direction, 176 vertical levels
- Timestep of 3 s, simulation up to 3 h

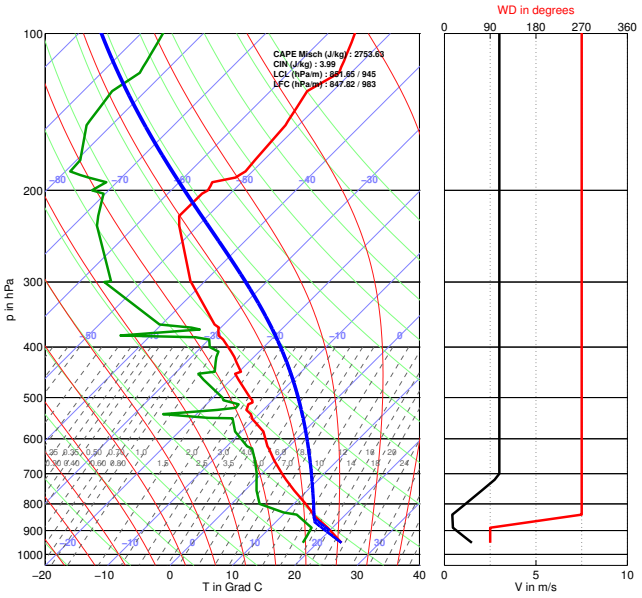

Fig. 3: Skew-T / log-p diagram of the initial profiles of temperature T in °C (red, left plate), dewpoint T_d in °C (green, left plate), wind direction in degrees (red, right plate) and windspeed in m s-1 (black, right plate) as function of pressure in hPa. Blue lines in the left figure: T of moist adiabatically lifted air parcels, one lifted from ground level, and one composed of mixed boundary layer air (lowest 100 hPa).

- Idealized initial and (fixed) lateral boundary conditions: profiles of temperature, moisture and wind speed as depicted in Figure 3. For these profiles, CAPE is about 2800 J kg^{-1}. These profiles have been synthesized from a sounding of 28/06/2006 near the city of Stuttgart, Germany (occurence of a strong hail storm) and nearby surface observations of temperature and dewpoint at the ground. Wind profile idealized adapted to the two-dimensional setup (i.e., $v = 0$)
- Initiation of a convective cell by constantly heating a bubble-like volume in the boundary layer during 15 min, leading to formation of a multicellular type storm system, beginning after about 25 min into the simulation.
- Nucleation of cloud droplets: look-up table for the initial cloud number concentration as a function of vertical velocity and aerosol properties by Segal and Khain (2006)
- Concerning ambient aerosol conditions, two cases: 1) low initial cloud droplet number concentration of about 100 cm^{-3} ("low CCN" case) and 2) large number concentration of about 1100 cm^{-3} ("high CCN" case).

In this paper, our studies on the properties of the two-moment scheme in the context of convective cloud simulations solely relie on the comparison of simulated radar reflectivity fields with commonly observed properties of the reflectivity profile for convective storms in a qualitative way. Radar reflectivity has been calculated from the modeled hydrometeor fields by methods described in Blahak (2007).

Referring to the simulations described above, Figure 4 depicts X-Z-cuts of simulated radar reflectivity along with isolines of temperature in °C after 50 min (upper row) and 100 min (lower row). For now, it is referred only to the left column which contains results obtained with the previous two-

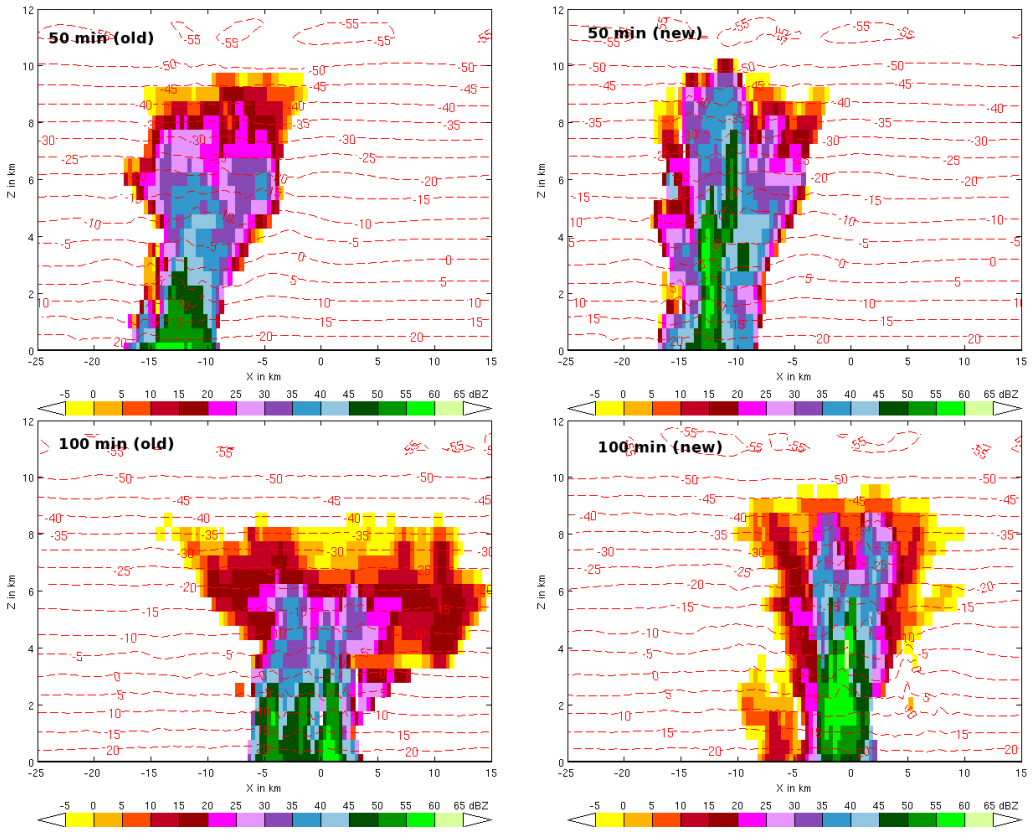

Fig. 4: X-Z-cuts of simulated radar reflectivity in dBZ for the high CCN case, after 50 min (top row) and 100 min (bottom row) simulation time, for the old updated version of the two-moment scheme (left column) and the newly updated version (right column).

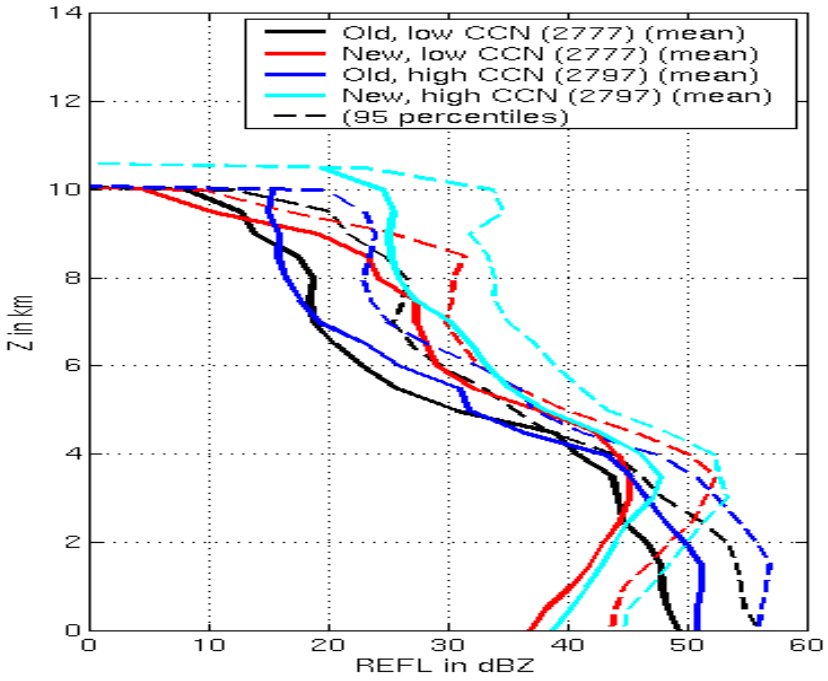

Fig. 5: Space-time-average profiles of reflectivity in dBZ as function of height in km. Averaging has been done in linear space and only gridbox values with a total Q exceeding 1×10^{-6} kg m^{-3} have been included in the average profile. Solid lines represent the actual average profiles, dashed lines show the corresponding 95-%-percentiles. "Old" denotes the previous version of the two-moment scheme, "New" the updated version. The 4-digit numbers in the legend are internal book-keeping codes denoting different settings of the scheme.

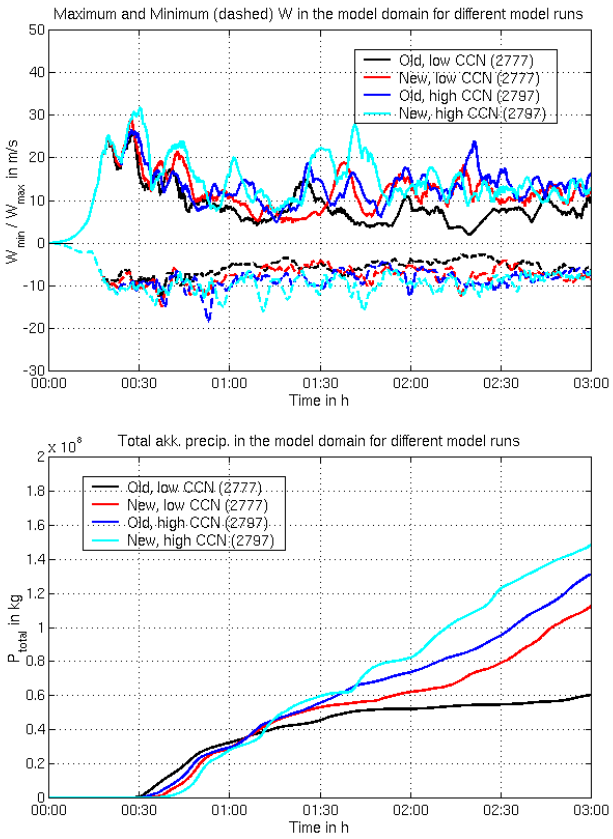

Fig. 6: Time series in h of maximum and minimum vertical velocity W_{max}/W_{min} within the model domain in m s^{-1} (top) and timeseries of total accumulated precipitation P_{tot} in kg (bottom). ***Note the factor 10^8 for $\mathbf{P_{tot}}$*** *values.*

moment model version (n the right side, results are shown after the further changes mentioned in the introduction (”new”), which will be described later). These reflectivity cuts (”old”) show a very typical feature which was observed in all simulations performed with the ”old” updated version: a very abrupt jump in reflectivity from very high values below the melting level ($>$ 50 dBZ) to rather low values above ($<$ 40 dBZ at $Z =$ 8 km). But radar observations of storms often show zones of high reflectivity (typically $>$ 50 dBZ and more) which reach up to heights of 10 km and above in midlatitude regions. These are commonly called ”reflectivity cores” and are probably connected to the presence of large ice particles (graupel and hail). This reflectivity deficit above the freezing level is consistently observed in all our other studies and is considered as a systematic behaviour of the 2-moment scheme.

To investigate the reflectivity profile in an average sense, conditional space-time-average profiles of reflectivity have been computed for the above simulations, i.e., horizontal averages over all grid boxes with Q exceeding a threshold of 1×10^{-6} kg m^{-3}. This reflects the average reflectivity where hydrometeors are present and rules out the influence of horizontal cloud extension as compared to horizontal domain averages. Figure 5 shows these profiles (blue and black solid lines for the ”old” version), along with 95-%-percentiles to indicate also the extremes of the space-time distribution of gridpoint values. It is obvious that the abovementioned jump in reflectivity (see blue and black solid line) at the melting level is observed not only for single timesteps but on average for the entire simulations.

It has to be mentioned that updraft speeds are rather low for the presented simulations and barely reach up to 15 m s^{-1} at later times of the simulation (see the upper part of Figure 6, blue curve for the high CCN case). The maximum updraft speed may be viewed as an indication of the overall vigorousness of vertical air motions within the storm, and may be a proxy for the amount of supercooled water and hail embryos present in the ice region, which initiate and support the growth of large particles. However, the apparently too low reflectivity in the ice region has been consistently obtained also for other simulations with higher updraft speeds.

As deeper analyses show, the explanation is, that just too many small particles are present so that riming growth of individual particles is limited by competition for the available supercooled water. To illustrate this, mass densities Q, number densities N and mean diameters D_M of the different hydrometeor classes are presented in the following. Again, conditional space-time-averaged vertical profiles of Q and D_M are utilized, i.e., horizontal averages over all grid boxes with Q and N exceeding thresholds of 1×10^{-6} kg m^{-3} and 1 m^{-3}, which shows the average mass density and size of hydrometeors where hydrometeors are present. These profiles for the above simulations are depicted in Figure 7 (Q) and 8 (D_M) for all 6 hydrometeor categories. Again, for now the focus is on the curves with label ”old” (black and blue). Solid lines are the space-time-average profiles and dashed lines show the corresponding 95-%-percentiles.

The following observations are drawn from these profiles:

- RIME-graupel and FRI-graupel particles (labeled as ”hail”) may be too small, and, since Q seems realistic, number concentrations may be too large.
- Strong increase of D_M of evaporating rain towards the ground, contributing to the sharp reflectivity jump near the melting layer.
- Strong increase of D_M of melting ice particles towards the ground, also contributing to the reflectivity jump.

These observations lead to major changes to the two-moment scheme which are discussed in the next section.

5 IMPROVING REPRESENTATION OF ICE PHASE PROCESSES

Motivated by the results presented in the last section, several modifications and extentions to the two-moment scheme have been made. These may be summarized as follows:

1) Particles of the same as well as of different ice species compete for available supercooled water, therefore, measures have been taken to decrease number concentration and (hopefully) increase particle size. These have been mainly changes to the mass-size- and mass-velocity- relations of ice, snow, and RIME-graupel. The previously discussed Figures 1 and 2 show a comparison of the previous (left column) and new (right column) bulk-density-size-relations (upper figures) and fallspeed-size-relations (lower figures) for all hydrometeor types. Main changes are:
(a) increased (spherical equivalent) bulk density of small cloud ice particles causing a decreased collision cross section and riming (decreased ice-to-graupel conversion)

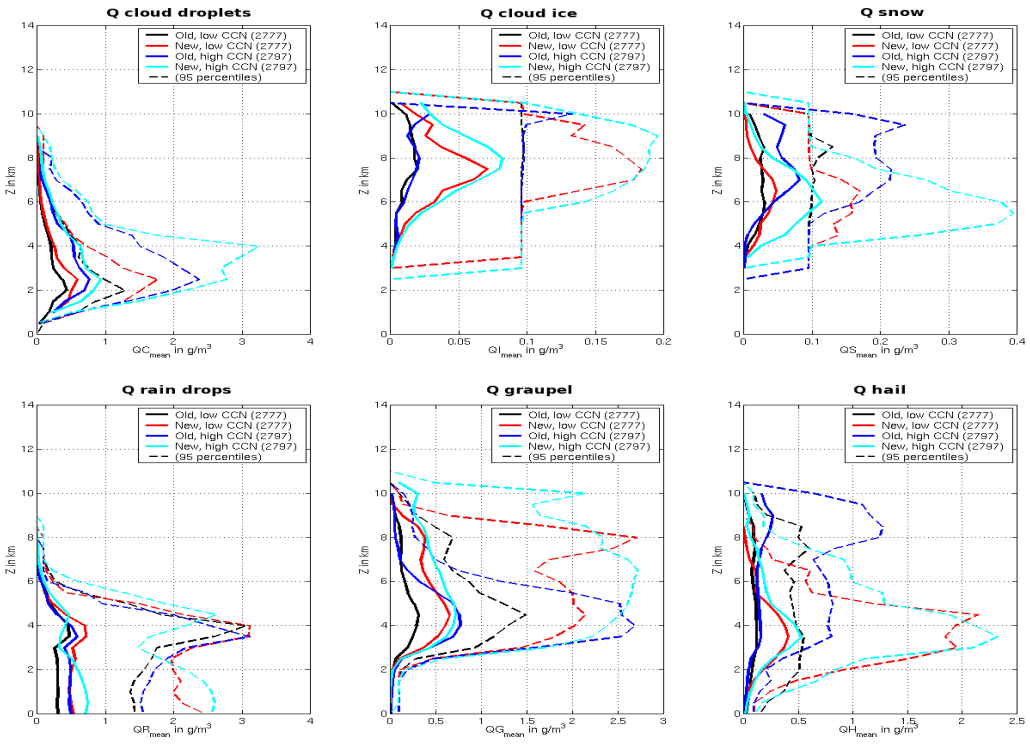

Fig. 7: Space-time-average vertical profiles of hydrometeor mass contents Q_x in $g\,m^{-3}$ of the 6 hydrometeor categories ($x \in \{c,r,i,s,g,h\}$, one plot for each category) as function of height in km. Averaged profiles include only those grid points with Q_x exceeding 1×10^{-6} $kg\,m^{-3}$. Different colors denote the different model runs (see legends of the plots). Solid lines are the actual mean profiles and dashed lines denote the 95-%-percentiles.

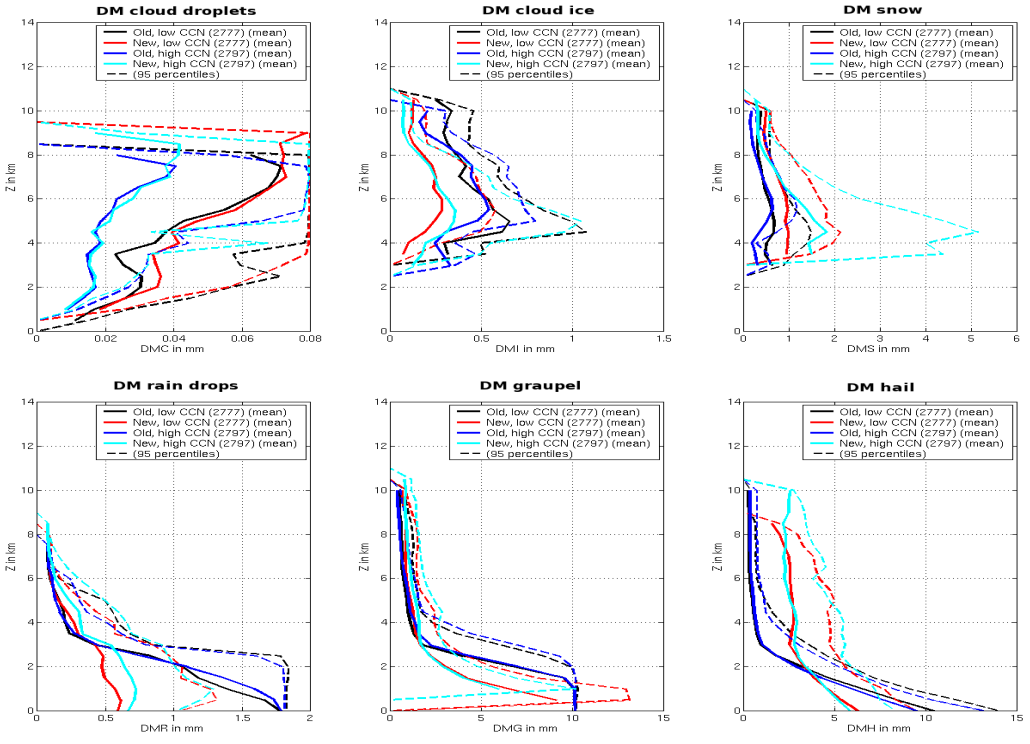

Fig. 8: Same as Figure 7 but for the mean mass diameter D_M. Only grid box values with $Q_x > 1 \times 10^{-6}$ $kg\,m^{-3}$ and $N_x > 1$ m^{-3} included in the mean profiles and the percentiles.

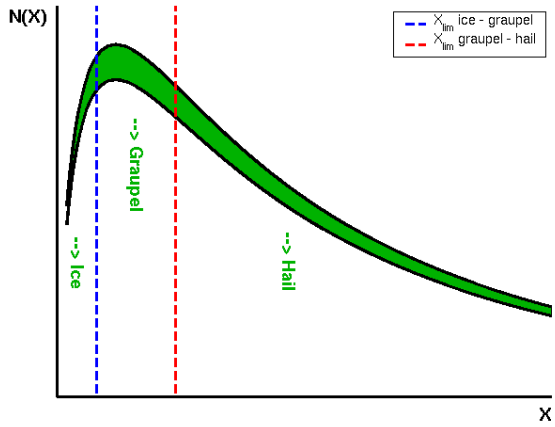

Fig. 9: Schematic diagram of spectral partitioning of freezing raindrops. See text for explanation.

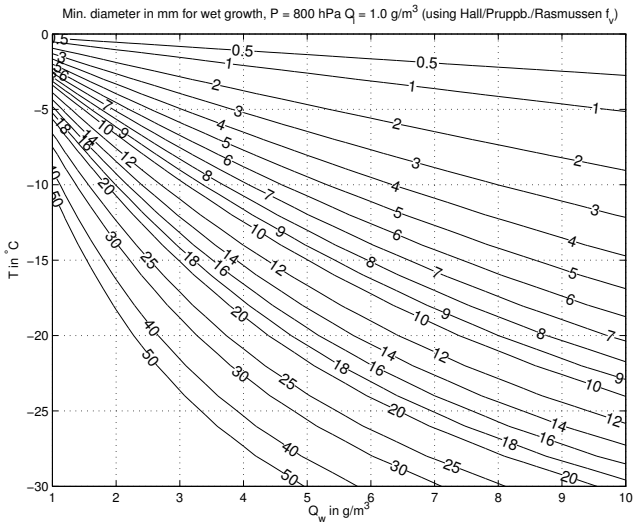

Fig. 10: Dividing diameter D_{wg} for wet growth regime in mm for the updated graupel category, as function of T in $^\circ$C, supercooled liquid water content Q_w in gm^{-3} and for an ice particle content $Q_i = 1$ gm^{-3}. Graupel particles having $D > D_{wg}$ are in wet growth mode. A pressure of 800ăhPa has been assumed here.

(b) Increased bulk density and fall speed of small graupel (increased riming of single particles)

2) Change with respect to the unrealistic behavior of D_M of rain: time rate of change of rain number concentration during evaporation now diagnosed based on the assumption of mean size conservation during evaporation, as is done in other schemes (e.g, Khairoutdinov and Kogan, 2000). The previously used parameterization of evaporative number concentration tendency had proven to be inappropriate.

3) Moreover, thoughts about the outcome of freezing rain have been stimulated. Does every freezing raindrop, "small" or "large", serve as an embryo for a high density ice particle? Considering that in a convective updraft ice hydrometeors also grow quite efficiently by depositional growth, mostly on the expense of supercooled cloud droplets (Bergeron-Findeisen-process), and if the conceptual model holds true that a very small initial ice particle may grow by deposition into a branched shape with lots of air inclusions inbetween (lower bulk density and fall speed), then it does seem inappropriate to treat every freezing raindrop as a solid ice sphere. Rather, the idea is now to split the outcome of freezing rain into ice, to lower- and to higher density graupel, according to raindrop size. This is now parameterized by a spectral partitioning approach: the rate of change of mass- and number concentration of raindrops is computed as before by integration of a mass (or size) dependent stochastic freezing probability over the (diagnosed) gamma-type raindrop mass distribution. Since the freezing probability is mass dependent, it is possible to split this integration into different parts according to threshold masses/sizes. Then, number and mass concentration of freezing raindrops in the size range from 0 to a first threshold size (say, $D = 0.5$ mm) are assigned to cloud ice particles. From there to a second threshold size, freezing drops are transferred to RIME graupel (larger initial ice particles do not attain as much air inclusions by depositional growth and retain a larger bulk density). Only those droplets with a size larger than this second threshold freeze into the FRI graupel category. A simple schematic sketch of this approach can be found in Figure 9: the sketched graph depicts the initial rain mass distribution at a certain gridpoint, diagnosed from rain N_r and Q_r. The green area is the part of it which freezes during one timestep. The part of the green area with mass smaller than the blue dashed threshold is converted to cloud ice, the part between blue and red to RIME graupel and the remainder to FRI graupel ("hail").

This technique seems to be beneficial in that it leads to larger mean size of FRI graupel, which resembles better the size aspect of the WMO definition of hail. Therefore the name "FRI graupel" is changed to "hail" in the following to indicate the now included size aspect. Consequently, "RIME graupel" looses its "RIME" suffix. This new freezing approach proofed to be beneficial in considerably increasing hail and graupel sizes aloft and in a better resemblance of the frequently observed reflectivity cores.

4) To further increase the hail-likeness of the hail category, the mechanism of conversion of graupel to hail by wetgrowth of graupel has been implemented (see section 2 for a description of the physical mechanism). The implementation is based on the calculation of D_{wg} (Schumann-Ludlam-limit) by means of the heat budget equation of individual high density ice particles, written as equation for the particle's core temperature T_s, as given by, e.g., Dennis and Musil (1973) and Nelson (1983), as well as on ventilation coefficients by Rasmussen, Pruppacher and Hall (Pruppacher and Klett, 1997). This equation predicts the time evolution of TS under the influence of latent heat release by riming, collection of other ice particles and turbulent heat exchange with the surrounding air. Important parameters are ambient temperature T, particle diameter, mass and fallspeed, as well as surrounding (supercooled) liquid water content and "accretable" ice content. Solving for a steady state and setting $T_s = 0^\circ$C leads to an equation for the dividing diameter D_{wg} for wet growth (see section 2). D_{wg} depends on T and pressure p (because of the fallspeed dependence of the accretion rate), on supercooled liquid water content and to a minor extent on the "accretable" ice- and snow content. Figure 10 shows isolines of D_{wg} for the updated graupel class as function of T and environmental supercooled water content Q_w. It is valid for $p = 800$ hPa

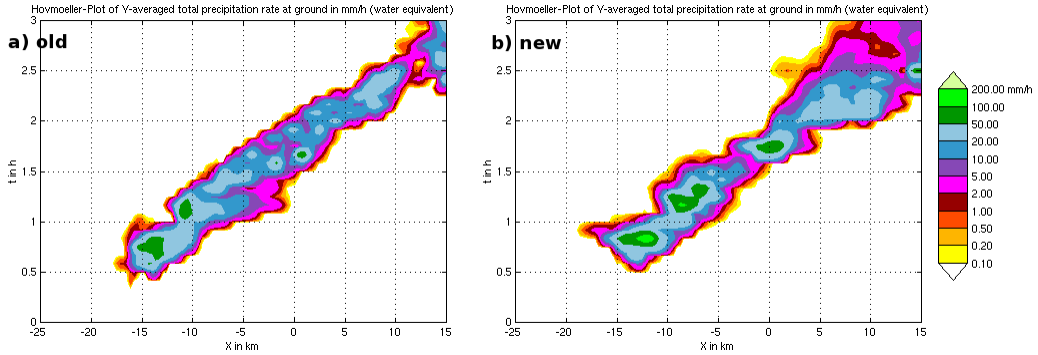

Fig. 11: Hovmoeller-diagram of total precipitation intensity at ground in mm h^{-1} as function of X in km and time in h, for the high CCN case. Previous verson of the two-moment scheme (left plate) and new version (right plate). Time runs from bottom to top.

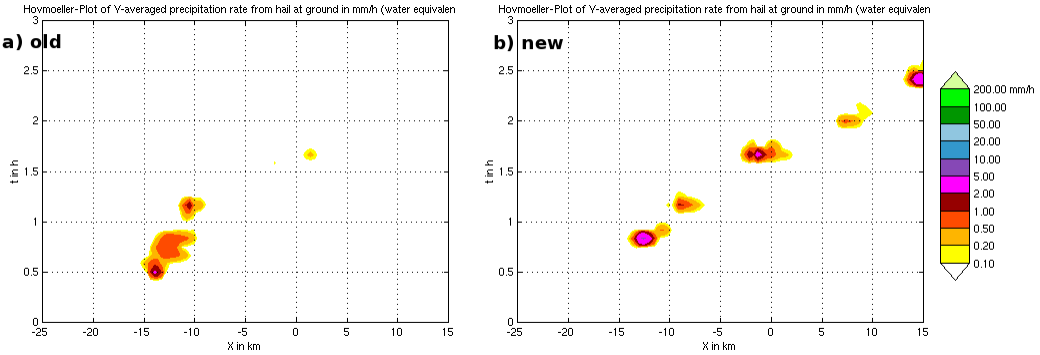

Fig. 12: Same as Figure 11, but for the hail only intensity at ground in mm h^{-1}.

and an ice content $Q_i = 1$ g m^{-3}. It can be seen that D_{wg} increases with decreasing Q_w and T. For $Q_w = 4$ g m^{-3} and $T =$ -10°C, D_{wg} equals 7 mm. D_{wg} as a function of the abovementioned 4 parameters is stored in a lookup table which covers the relevant range of atmospheric conditions.

Parameterization of wet growth conversion from graupel to hail is again based on a spectral partitioning approach, as for the abovementioned partitioning of freezing rain drops. For each grid box and at each time step, DWG is diagnosed using a precalculated lookup table, and based on this threshold and if graupel is present, the part of the (diagnosed) graupel size distribution exceeding the threshold, or more specifically, mass and number concentration contained therein, are converted into hail. This constitutes a further source for large hail particles.

5) To address the issue of strongly increasing mean diameters of melting ice particles towards the ground, the time rate of change of number concentration during melting is now diagnosed also in a way that mean size of the ice species is preserved. Similar parameterization issues as compared to treatment rain number concentration during evaporation have been responsible for the apparently wrong behaviour. The above solution, however, is only regarded as an intermediate practical solution, until a better way has been found, probably based on the explicit prediction of the melted fraction in conjunction with a proper shedding parameterization for large graupel and hail particles.

The version of the bulk scheme which comprises all abovementioned changes will be called the ”updated version”. The overall effect of these changes is depicted in Figures 4 to 8, 11 and 12: Figure 4 shows X-Z-cuts of simulated radar reflectivity after 50 min and 100 min (high CCN case) for the previous (”old”) and updated version (”new”) of the two-moment scheme. Figure 6 compares timeseries of maximum and minimum vertical velocity in the model domain and total accumulated precipitation. Also shown are conditional space-time-averaged vertical profiles of simulated reflectivity (Figure 5), of hydrometeor mass densities (Figure 7) and mean mass diameters (Figure 8). Finally, precipitation rate at the surface as function of time is presented as Hovmoeller-Plots in Figure 11 (overall precipitation rate) and Figure 12 (hail only).

Observations and results can be summarized as follows:

- After changes to the scheme: now we get bigger hail particles aloft. The main effect is caused by introduction of spectral partitioning in raindrop freezing parameterization. The graupel mean size is only marginally larger.
- Parameterization of graupel-to-hail conversion due to implementation of wet growth acts as further source for large hail particles.
- More hail reaches the ground due to increased size and fallspeed.
- Due to the presence of larger hail aloft, now reflectivity cores are simulated more realistically.
- Vertical profiles of mean particle size D_M are more plausible since now D_M of rain, graupel and hail does not increase as much towards the ground as before.
- Increased precipitation in both the low-CCN and high-CCN cases. Interestingly, the high-CCN clouds overall produce more precipitation in this case due to longer cloud lifetime.

The reason for the longer lifetime has yet to be determined and may either be due to stronger secondary cell generation by stronger coldpools (stronger evaporation of smaller raindrops) or due to enhanced latent-heat-of-freezing-release due to less active warm rain processes.

For an even more realistic parameterization of hail, one would need to incorporate a parameterization of shedding along with the prediction of the liquid water fraction for the hail category. This would enable a better parameterization of melting and refreezing, important for the recirculation process, and also would improve the calculation of radar reflectivity.

6 CONCLUSIONS

The two-moment bulk microphysical scheme of Seifert and Beheng (2006) including an additional particle category of high density (FRI-)graupel particles (Noppel et al., 2006) has been qualitatively assessed concerning the simulated reflectivity structure in convective clouds. It has been found that especially the often observed high reflectivity values in the upper central part of active convecitve clouds, forming the socalled reflectivity cores, cannot be adequately simulated by this version of the scheme. Rather, a systematic feature of the simulated reflectivity field is a distinct jumplike drop from reflectivites below to above the freezing region. As analyses of the mean particle sizes (defined as the ratio Q/N transferred to an equivalent diameter) show, this is behaviour is due to very small particles in both graupel categories (dominating particles in convective updrafts), associated by very high number concentration. In this case, particle size is the dominating factor contributing to reflectivity.

Therefore, the parameters of size-mass- and velocity-mass-relations of all ice categories have been changed in a way that less RIME-graupel particles initiate by riming, which then can grow bigger by further riming because there is less competition for the available supercooled water. In addition, the initiation of high density FRI-Graupel by freezing of raindrops has been changed. Before, all freezing raindrops were converted to FRI-graupel. Now only particles exceeding a certain size threshold initiate to FRI-graupel, all others are converted either to cloud ice (very small raindrops) or to RIME-graupel. Again, this leads to fewer but larger particles. Further, to render the FRI-graupel more "hail-like", the conversion of RIME- to FRI-graupel by the socalled wet-growth process has been implemented. RIME-graupel will be called "hail" from now on. However, for a realistic simulation of certain hail formation processes (e.g., melting $\rightarrow$ recirculation $\rightarrow$ refreezing), better treatment of melting and shedding is needed, probably including the prediction of the water fraction of melting particles.

All these measures lead to a more realistic simulation of high reflectivity values in the upper part of convective clouds, and there is also an increase of the precipitation efficiency due to stronger sedimentation of the now larger graupel and hail. However, the arguments leading to the model changes are mostly based on qualitative and sometimes intuitive "backwards guessing" from common radar observations, due to lack of proper in situ observations of particle properties within strong convective updrafts. Further verification by real case studies and comparison to a detailed bin microphysics model (Hebrew University Cloud Model) is currently under way.

REFERENCES

Blahak, U., 2007: RADAR_MIE_LM and RADAR_MIELIB — calculation of radar reflectivity from model output, *Internal report, Inst. f. Meteor. and Climate research, University/ Research Center Karlsruhe*, available on request.

Dennis, A. S. and D. J. Musil, 1973: Calculations of hailstone growth and trajectories in a simple cloud model, *J. Atmos. Sci.*, **30**, 278–288.

Khairoutdinov, M. and Y. Kogan, 2000: A new cloud physics parameterization in a large-eddy simulation model of marine stratocumulus, *Mon. Wea. Rev.*, **128**, 229–243.

Nelson, S. P., 1983: The influence of storm flow structure on hail growth, *J. Atmos. Sci.*, (40).

Noppel, H., U. Blahak, K. D. Beheng and A. Seifert, A two-moment cloud microphysics scheme with two process-separated modes of graupel, 12. AMS Conference on Cloud Physics, 10. – 14.7.2006, Madison, Wisconsin, available online: http://ams.confex.com/ams/pdfpapers/113532.pdf, 2006.

Pruppacher, H. R. and J. D. Klett, *Microphysics of Clouds and Precipitation*, Kluwer Academic Publishers, Dordrecht, Boston, London, 1997, 2. edition.

Segal, Y. and A. Khain, 2006: Dependence of droplet concentration on aerosol conditions in different cloud types: Application to droplet concentration parameterization of aerosol conditions, *J. Geophys. Res.*, **111**, D15204, doi:10.1029/2005JD006561.

Seifert, A. and K. D. Beheng, 2006: A two-moment cloud microphysics parameterization for mixed-phase clouds. part I: Model description, *Meteorol. Atmos. Phys.*, **92**, 45–66.

Seifert, A., A. Khain, A. Pokrovsky and K. D. Beheng, 2006: A comparison of spectral bin and two-moment bulk mixed-phase cloud microphysics, *Atmos. Res.*, **80**, 46–66.

Young, K. C., *Microphysical Processes in Clouds*, Oxford University Press, 1993.